SCA2003-21

VISUALIZATION OF THREE PHASES IN POROUS MEDIA USING MICRO COMPUTED TOMOGRAPHY

Freddy E. Alvarado, Abraham S. Grader, Ozgen Karacan, Phillip M. Halleck.
The Pennsylvania State University-Energy Institute and Department of Energy and Geo-Environmental Engineering

ABSTRACT

Three-phase flow in porous media is a common phenomenon in hydrocarbon reservoirs. This study presents quantitative maps of fluid distribution in a granular porous medium using micro computed tomography (MCT). The study was done in an effort to determine the position, distribution and saturation of each phase at the pore-scale level. Quartz sand was used as the porous media. The fluids used were water (doped with NaI), benzyl alcohol (BA) and decane (doped with iodo-dodecane). The three fluids and the solid phase were mapped in images that were acquired at a single energy setting. Single-phase, two-phase and three-phase saturation distributions were developed. The intermediate phase was detected by direct observation of the phase distribution in the porous medium thus confirming calculations using interfacial tensions and the spreading coefficient.

The results obtained from this research showed that micro computed tomography (MCT) is a useful technique to study multi-phase flow mechanisms in porous media. This work provided three-dimensional maps of fluid saturations at the pore level and should allow the reconsideration and adjustment of pore-scale modeling. This method provides the possibility to obtain three-dimensional saturation data that can be used for simulator development and calibration of models.

INTRODUCTION

Understanding multi-phase flow in porous media is essential for optimizing hydrocarbon recoveries from oil and gas reservoirs. Three-phase flow occurs in many hydrocarbon recovery processes such as in solution gas drive, gas cap expansion, alternating water and gas injection, and gas or steam injection. Pore occupancy of each phase has a strong influence on relative permeabilities and is a reflection of capillary and gravitational forces. Therefore, it is essential to understand phase distribution in the reservoir in order to develop appropriate predictive models.

Until recently, the visualization and analysis of the flow behavior at the pore-scale had been realized using transparent two-dimensional glass models where fluid flow could be observed. Due to lack of space, only a few references are included. One of the first pore-scale studies, Kimbler (1957) [1], presented a photographic approach used to analyze two-phase flow displacement in a glass sample, during the injections of two immiscible fluids along the glass. The results of that experiment showed low-resolution fluid distribution in the core at different times. The distribution of multi-phases in pores has been considered by many authors including Kantzas and Dullien (1988) [2,3]. They

applied the concept of aspect ratio and capillarity to oil recovery processes using inert gas injection.

Howard et al. (1993) [4] performed a pore-scale study using proton nuclear-magnetic-resonance method (NMR) with a spatial resolution of about 200 microns, allowing the visualization of some inter-granular pore spaces. They proposed that the permeability of a sample depends on the porosity and a magnetic relaxation time. Jasty et al. (1993) [5] presented two-dimensional images of oil and water phases in pores, thus demonstrating the applicability of MicroCT to quantitative visualization of pore-scale multi-phase flow studies. Oren and Pinczewski (1995) [6] presented a description of the fluids distribution and pore-scale mechanisms for three-phase flow (2D model). In this experiment the study was developed in a glass micro-model evaluating many different conditions of fluid-rock wettability. Rosenberg et al. (1997) [7] presented a high-resolution x-ray study on rocks. They used a microscanner with an electron microprobe as a "point x-ray source" that allows a standard resolution of about 10 microns. The quality of the acquired microscanner data was confirmed by a SEM images.

Al-Sharji et al. (1999) [8] presented a visual interpretation of the displacement of oil and water by a polymer gel at the pore-scale level. The experiment was conducted in a transparent glass model. The results were recorded with a microscope and camera. The pore size of the network varied form 60 to 250 microns. They showed from visual characterization that the polymer gels reduced water permeability more than oil permeability. Oren and Picnzewski (1995) [6] have shown, using a micro glass model, that three-phase relative permeabilities are particularly governed by pore-scale effects, and that the fluid morphology has a significant influence on the mechanism of displacement.

In cases where the porous medium is strongly wetted by one of the phases the other two phases are considered non-wetting. However, one of these non-wetting phases is aligned between the two other phases and is denoted as the intermediate phase. The least wetting phase usually occupies the large pores. The identity of the intermediate phase is determined by the fluid-fluid interfacial tensions. As an example, in the presence of water, oil, and gas in a water wetting system, the water may be located in the smallest pores. Between the two non-wetting phases, it is needed to determine which phase occupies the large pores and which is the intermediate phase. In a water-wet system, if $\sigma_{gw} > \sigma_{ow}$, oil will be the intermediate phase, leaving the large pores for the gas. Dullien (1996) [9] presented an equation relating the spreading coefficient to the interfacial tensions between pairs of two phases that, defines the intermediate phase:

$$S_{intp} = \sigma_{wp\text{-}nwp} - \sigma_{wp\text{-}intp} - \sigma_{intp\text{-}nwp} \quad (1)$$

S_{intp} denotes the intermediate phase spreading coefficient, $\sigma_{wp\text{-}nwp}$ represents the interfacial tension between the wetting phase and the non-wetting phase, $\sigma_{wp\text{-}intp}$ represents the interfacial tension between the wetting phase and the intermediate phase, and $\sigma_{intp\text{-}nwp}$ represents the interfacial tension between the intermediate phase and the non-

wetting phase. The intermediate phase is determined when the spreading coefficient is positive. The wettability of the rock is a characteristic that depends not only on the mineral composition of the rock but also on the composition of the fluids.

The effect of wettability on the three-phase relative permeabilities has been studied by many researchers. Van Dijke (2000) [10], Dicarlo et al. (2000) [11], among others, have studied the influence of the wettability for a water-wet, oil-wet, and mixed–wet cases using different approaches. However, the verification of the intermediate phase in a porous medium has not been presented in the literature. There is a lack of experimental data of the three-dimensional pores-scale distribution of the three phases in porous media. This lack includes static and dynamic experiments. The experimental results presented in this study are essential for understanding the fluid flow mechanisms that determine the fluids transport process.

EXPERIMENTS

Computed Tomography and X-Ray CT Scanner

X-ray Computed Tomography is a non-destructive technique for mapping the internal distribution of the density and atomic numbers of an object. It was originally developed in Great Britain by Hounsfield in 1972 primary for medical purposes. This technique is used today in industrial application under the category of non-destructive evaluation, NDE. Computed Tomography has been used in the oil industry since 1980's (Wang et al., 1984 [12], Wellington and Vinegar, 1987 [13], Hicks et al., 1992 [14], Grader et al., 1998) [15]. One of the most recent work on the effects of gel injection on fluid flow in sandstones and simulated cores was presented by Seright et al. (2002) [16]. They reported pixel resolutions of 4.1 microns and were able to determine two-phase distributions, pore sizes, and aspects ratios in the samples.

Computed Tomography has been used to study fluid flow in rock samples and for detailed characterization and screening cores. This technique is base on the attenuation of x-rays passing through a sample. X-ray sources are made in a range of acceleration voltages and applied currents. The penetration ability of x-rays depends on the voltage while the current determines how many photons are generated at a specific voltage. Small focal spots at the x-ray sources provide better resolution. However, it is difficult to make high voltage and high current x-rays to emit from a small focal spot. This study used a micro-focus x-ray source at 145 kV and 1000 μA with a focal spot about 5 microns. The voxel resolution for the work presented here was about 9 microns, a resolution sufficient for imaging the pores in the sample.

The industrial (OMNI-X) CT unit used is a third generation scanner where the source and detector are fixed and the scanned object rotates. The system has a 225 kV micro-focus x-ray generator and a 225 mm diameter image intensifier. The micro-focus x-ray source allows high magnification by placing the object near the x-ray source. The highest resolution that can be obtained by the micro-focus source is about 5 microns. Once the object is brought to its position and the scanner is activated, the projections of the

magnified object are captured by the image intensifier. When the source is active, the x-rays penetrate through the object and reach the image intensifier, which converts x-ray energy into a form of light that is captured by a digital video camera. The digitized data are sent to a computer and turned into raw files that can be processed into images.

High-resolution images have1024x1024 pixel elements, giving a total grid of 1,048,576 individual pixels per image. As the object rotates in the x-ray beam the detector records the attenuated signal periodically. These recordings are called views and the resulting records can be used to construct single or several slices in one rotation. When several images are reconstructed from one rotation the system is in "volume mode" producing a volume representation of the sample. A single rotation of 360 degrees in this study consisted of 2400 views. Precise movement and high-level magnification are essential for this study since fluid observation at the pore-scale is required.

Core Holder

The sample holder consisted of a glass tube containing loose sand. The tube had an outer diameter of 9 mm, an inner diameter of 7 mm, and a length of 120 mm giving a total bulk volume of 10.8 cc. The porous medium consisted of non-spherical quartz sand with an average grain size was about 1 mm. Sequences of images were acquired at exactly the same position so that image subtraction can be used as part of the analysis procedure. The core holder was designed to keep the core centered while rotating in the CT unit, and to allow the fluids to pass through it from bottom to top. The location of the grains in the system did not change during the injection of the fluids, thus, once grain positions were determined they were eliminated from all images. At high-magnification, any movement of the core can result in loss of the original position of the object and therefore a failure of the experiment. Figure 1 shows the core holder during the injection and scanning processes.

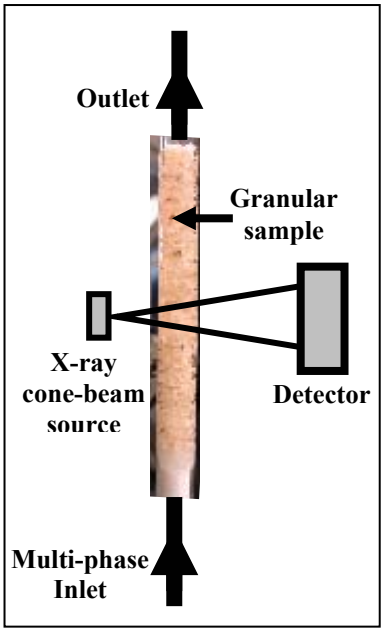

Figure 1: Experimental Schematic.

Fluids and Injection System

The three fluids used for this experiment were water, benzyl alcohol, and decane. For each phase, the CT values, which are a combined measure of the density of the object and its mean atomic number, were recorded. In order to differentiate all the phases in the system, it was necessary to tag the fluids with tracers. The wetting phase (water) was doped with NaI, and its CT number was measured using different concentrations. Following the same procedure, decane was doped with iodo-dodecane, testing different concentrations until a clear contrast among the phases was obtained. The benzyl alcohol was not tagged. The three fluids were pre-mixed to achieve chemical equilibrium. Table 1 provides a reference value of the fluid properties.

Table 1: Fluids Properties (Al-Wadahi, 1996).

Fluid	Density (g/cc)	Dynamic viscosity (cp)
Water	1.0377	1.1534
BA	1.0265	5.0563
Decane	0.7416	0.9659

METHOD

The glass tube was filled with quartz sand and the grains were compacted in such a way to avoid movement during the vacuum, flooding, or scanning processes. The grains were packed by vertical tapping while applying pressure to the upper free sand interface. Once the core was packed, two plugs were attached to the glass tube, and then connected to the teflon tubing. The core was placed in the core holder and positioned in the scanner. The first high-magnification scanning sequence was acquired under a vacuum condition in order to have the dry pore space as a reference. After scanning, the core was saturated with water and it was re-scanned. Then oil was injected displacing the water until residual water saturation was obtained. Two- and three-phase injection periods followed the initial oil flood.

First Stage:

Once the images were obtained they were cut to eliminate the unwanted regions beyond the edges of the sample. The center of each image was identified and then, using the known radius the image was cropped to a square with each side representing the diameter of the sample, and all external pixels were arbitrarily changed to a fixed value. The cropping process reduces the size of the images and makes all future manipulations more efficient than if the original size was used. For this study an original matrix of 1024x1024 was reduced to a size of 770x770. Figures 2A and 2B show a comparison of a typical image before (A) and after cropping (B).

Second Stage:

After cutting and masking the data, the next step was to partition the dry scans. The dry scans form the base for computing the porosity of the sample. In this stage the image voxels were partitioned into two groups, solid and pore. Since the interfaces between materials are not step functions but S shaped, a threshold is needed to distinguish the objects. Different thresholds were applied in order to separate rock and air. A proper threshold was selected so that the grains have points of contact with each other in the three-dimensional space. In a typical image the grains appear to be “floating” and not connected. Since the sand is unconsolidated, there are very few points of contact between the grains. The high-resolution images cover the entire volume making it possible to find most of these contact points and to preserve them by proper thresholding. Figure 2 shows an example of an original (A) and the same image after partitioning (C) where the solid is denoted by white and the pore space by black. The colors are arbitrary. The definition of the solid phase is strictly preserved for all images that contain fluid in later experimental stages.

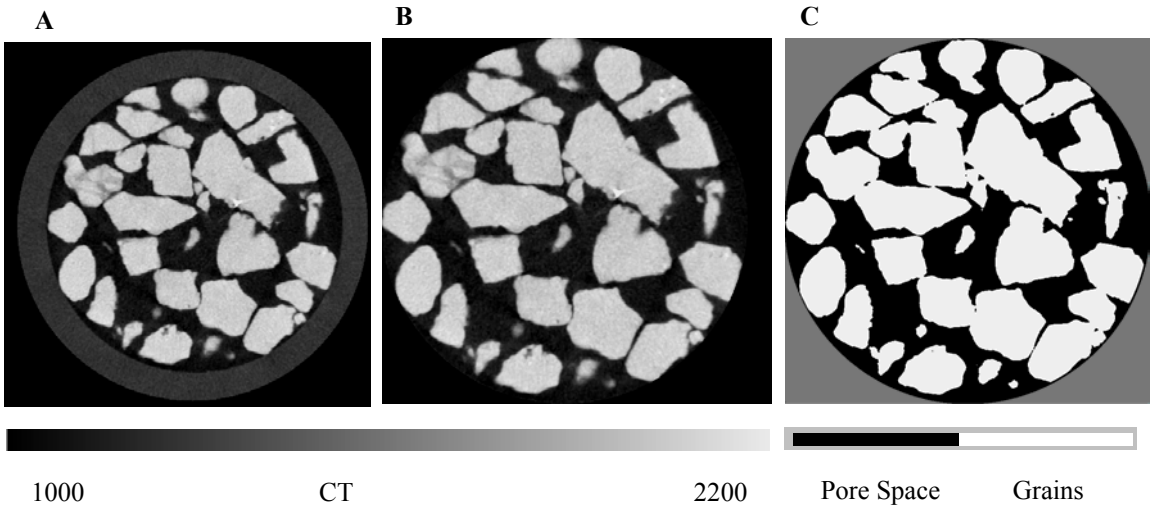

Figure 2: Example of processing an image of the dry core. A: original. B: cut. C: partitioned.

The masking process allows the identification and the location of the grains. The partitioning algorithm was applied to the dry images. Thus, since there were no other phases in the system the pore space was identified. The porosity is defined as: $\phi=V_p/V_b$ where V_p is the pore volume and V_b is the bulk volume. The porosity of each image can then be computed by dividing the sum of the pore space pixels by the sum of the pixels that represent the grains plus the pore space. Thus, an average porosity profile along the scanned region was created and the overall average porosity was computed. After the dry scanning sequence the core was saturated with water and was scanned. The sequence of images corresponding to the fully water-saturated core ensures that there is no air in the system prior to the benzyl alcohol flood. However, it does not provide more information than the sequence of dry scans.

Third Stage:
This stage focused on partitioning fluid occupancy in multi-phase scans. There are three types of scans that required special considerations: two-phase at static conditions, three-phase at static conditions, and three-phase at flowing conditions. All the processing presented in this study was centered on the first two conditions. The processing and analysis of the third condition (three phases under dynamic condition) is under analysis and is beyond the scope of this paper.

After the drainage process, a sequence of scans was acquired at the end of the benzyl alcohol flood. The resulting images were reduced in size and then the grains were subtracted using the grains mask. Thus, only residual water and benzyl alcohol are left with direct non-processed CT values. The water has a high CT number in comparison to the BA, thus allowing the partitioning of the two phases. Figure 3 shows a sample

slice. The grains are denoted by the dark gray, water by white color, and benzyl alcohol by gray. The water, being the wetting phase, occupies mainly the small pores. The saturations of the fluid can be computed directly by dividing the numbers of pixels representing the fluids by the number of pixels representing the pore space. The MCT cannot detect the wetting water phase around the grains in non-contact areas. Therefore, oil appears to surround most of the grain surfaces shown in Figure 3.

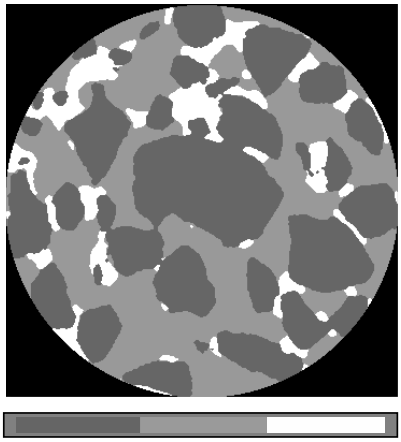

Figure 3: CT image at residual water saturation.

The computation of the three-phase fluid saturation was a more difficult procedure than for the two-phase case. Since the interface between the fluid-fluid and fluid-rock was not sharp, edge effects must be considered. The CT number of the decane is between the CT of the water and the benzyl alcohol, creating a challenge to the partitioning process.

Porosity

Typical dry views of the sample are shown in Figure 4 (right). The slice at the upper left shows the core with glass core holder tube. The three white dashed lines represent vertical planes that are presented below and to the right of the image. The resolution in x-y-z is 9x9x21 microns. The single image in the upper left is a 1024x1024 reconstruction with a pixel resolution of 9x9 microns. The axial resolution is 21 microns. Most of the grains appear "floating" without contacts for each grain. However, as all the images are explored there are at least three points of contact to most of the grains. There are a total of 410 slices, spanning a length of 8.59 mm. A vertical porosity profile along the sample is presented in Figure 4 (right). The local porosity (per slice) is variable over the image and between images, and is strongly affected by grain sizes. The average total volume porosity of the volume is 0.48.

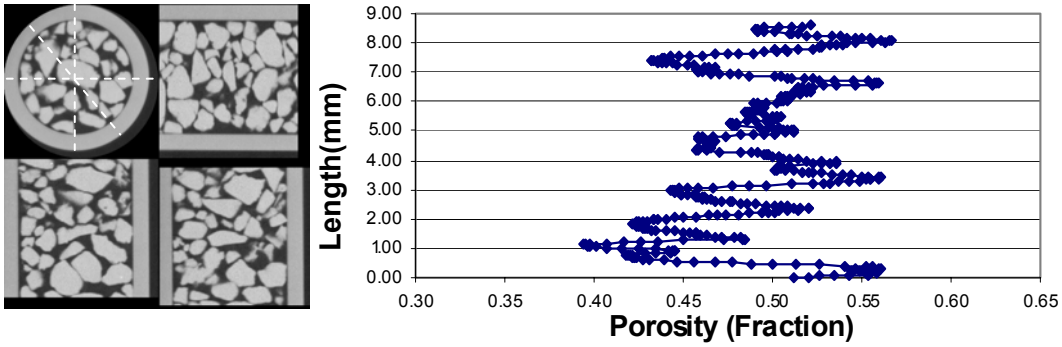

Figure 4: Axial and transverse cross-section of the dry core (left) and porosity vs axial position (right).

Sharp changes in the local porosity are observed due to the high axial resolution. The large changes in the porosity Figure 4 (right) are attributed to the fact that each slice is 21 microns thick. Thus, a grain of about 1 mm in length requires 50 slices to describe its entire volume. The presence of a few large grains causes large changes in porosity.

Two-Phase System

A plate of twelve consecutive images at residual water saturation is shown in Figure 5A where water is next to the grains and oil occupies the large pore spaces. Although the small pores are mainly filled with water, in a single slice there are some places in which water appears to reside in large open pores. This appearance is attributed to the two-dimensionality of each slice and underscores the need to examine the CT data in three-dimensions. The sequence of images in Figure 5A show that the strip of water below the circled grain is held in place by capillary forces created by a neighboring grain that is not visible at the level of the first image in the sequence.

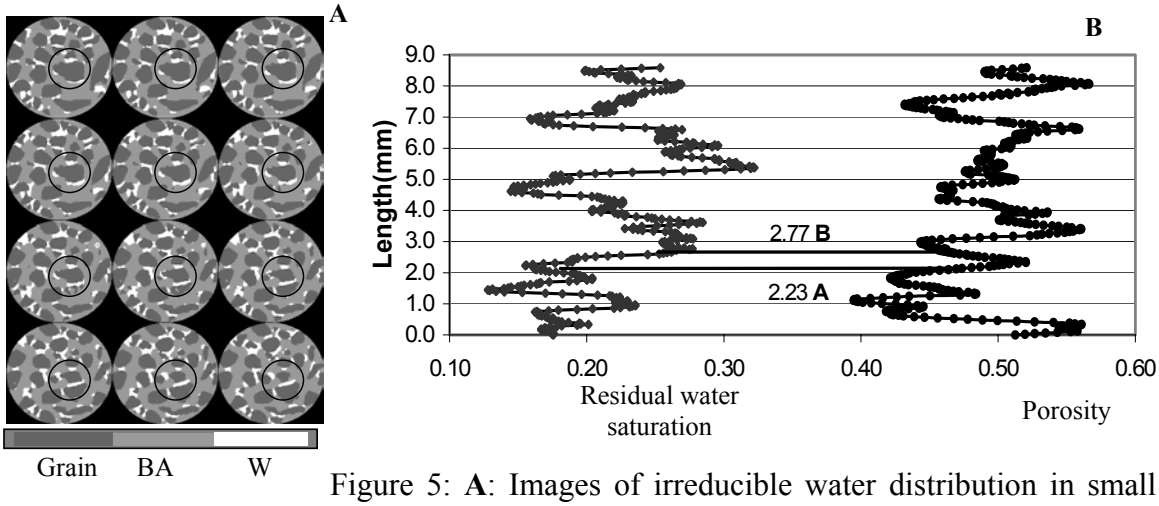

Figure 5: **A**: Images of irreducible water distribution in small pores. **B**: Irreducible water distribution along the core.

From a granular porous media we typically expect an inverse relationship between porosity and residual saturation of the wetting phase (mainly water in this case) No relationship between residual water saturation and porosity was found. The size of the grains in the experiment was large in comparison to the diameter of the sample. Hence, it was not possible to select a representative elemental volume (REV). The actual grain size distribution for the entire scanned sample is needed to relate averages of saturations to porosity and grains size. Figure 5B highlights a specific incremental change in residual water saturation between 2.23 and 2.77 mm from the bottom of the scanned portion of the sample. The increase in residual water saturation in the upward direction corresponds to a decrease in pore space.

Three-Phase System

After the injection of benzyl alcohol reduced the water saturation to its irreducible level, benzyl alcohol and decane were injected simultaneously at fixed ratios. Two injection ratios of 2:1 and 1:1 decane to benzyl alcohol were used. After the first injection sequence, the sample was isolated and scanned. The presence of the third phase in the system produces spreading. Figure 6A presents an example of how the intermediate phase (benzyl alcohol) spreads over the wetting phase as a consequence of the interfacial tension. The prediction that the intermediate spreading phase in this three-phase system is benzyl alcohol (based on interfacial tensions, Al-wadahi, 1994) is confirmed in Figure 6. Figure 6B shows the CT profile that identifies grains (1), decane (2), benzyl alcohol (3), and water (4).

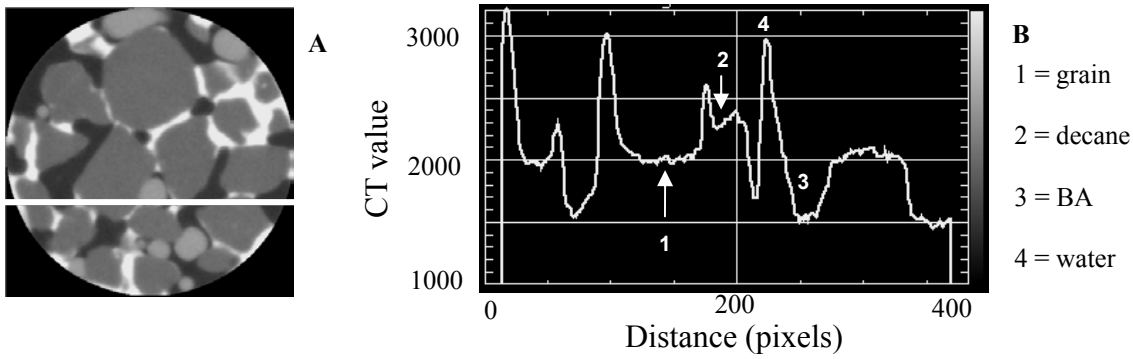

Figure 6: **A**: Image including the three phases. **B**: Linear profile highlighting that BA is the intermediate phase.

Figure 7 shows a partitioned three-phase system. Water is represented by white, decane as light gray, benzyl alcohol as dark gray, and the grains are black. Although all three phases are present, water is at irreducible saturation. The injection of the decane and oil at this specific ratio did not displace additional water. The small pores are still occupied by the wetting phase, water. The decane, as a non-wetting phase, occupies the large pores, leaving benzyl alcohol as the intermediate phase. Figure 7 also highlights a single decane bubble surrounded by benzyl alcohol, thus confirming that it is the intermediate phase.

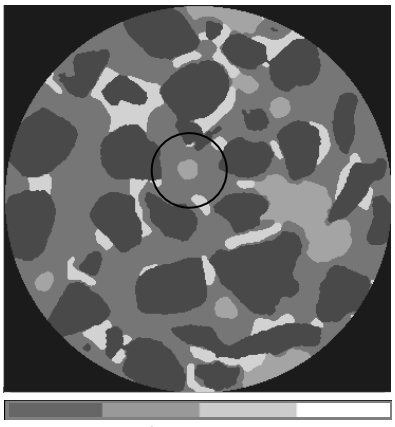

Figure 7: Image of three phases after partitioning.

The group of partitioned images serves as the basis for creating three-dimensional views of each of the phases in the system: water, benzyl alcohol, decane, and solids. Figure 8 presents three-dimensional views of the three phases in the system. Water is at residual saturation and is the wetting phase in the system. Its three-dimensional shapes are

associated mainly with grain contacts. The benzyl alcohol is the intermediate phase and is at high saturation and is adjacent to the large portion of the population of grains. MCT cannot detect thin water layers that are probably present around most of the surfaces of the grains. The decane is the least wetting phase and forms ganglia within the large pores of the sample. Some of the bodies are spherical in shape, and some form elongated shapes that span several pores. Three-dimensional renderings of the pore space and the solid are shown in Figure 9. Knowledge of the pore space structure enabled the determination of local and overall porosity values and saturation levels.

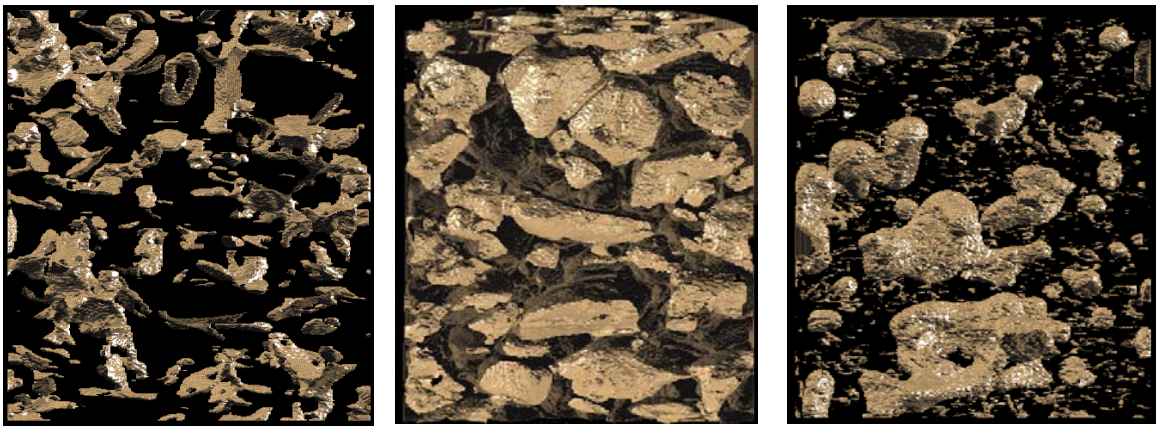

Irreducible water Benzyl alcohol Decane

Figure 8: Three-dimensional views: Left: water, Middle: benzyl alcohol, Right: decane.

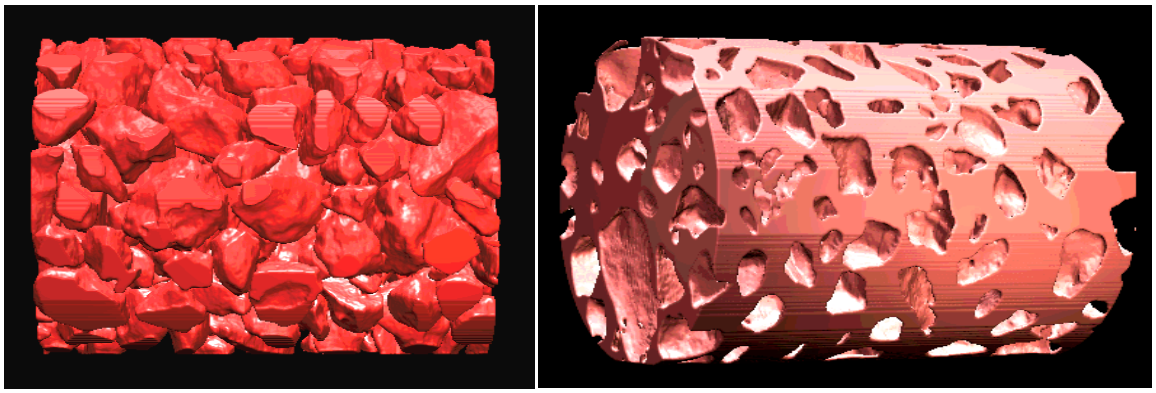

Figure 9: Three-dimensional views: Left: solids, Right: pore space.

CONCLUSIONS

Computed Tomography (CT) is a viable technique to study the distribution of three phases at the pore scale level non-destructively. The quantification of the saturations of each phase in two- and three-phase systems using MCT is a technique that can be applied at non-synthetic models to understand the fluids behavior at the pore-scale. Three-dimensional distributions of the three phases in the pore system were obtained. A three-dimensional pore structure was obtained using MCT. This pore structure could be used as the basis of developing a network model. The definition of the intermediate phase was made by direct observation of CT images, confirming early computations of the spreading coefficient.

REFERENCES

1. Kimbler, O. K. and Caudle, B. H., “New technique for Study of Fluid Flow and phase distribution in porous media,” The Oil and Gas Journal, vol.55, 85-88, December 1957.
2. Kantzas, A., Chatzis, I. and Dullien, F.A.L., "Mechanisms of Capillary Displacement of Residual Oil by Gravity Assisted Inert Gas Injection", SPE 17506, Proceedings, SPE Rocky Mountain Regional Meeting, Casper, Wyoming, May 11-13, 1988.
3. Kantzas, A., Chatzis, I., and Dullien, F.A.L., "Enhanced Oil Recovery by Inert Gas Injection," SPE 17379, Proceedings, SPE/DOE Symposium of Enhanced Oil Recovery, Tulsa, Oklahoma, April 17-20, 1988.
4. Howard, J., Kenyon, W. E., and Straley, C., “Proton Magnetic Resonance and Pore Size Variations in Reservoir Sandstones,” SPE Formation Evaluation, 194-200, September 1993.
5. Jasty J. K., Jesion, G., and Feldkamp, L., “Microscopic Imaging of Porous Media With X-Ray Computer Tomography,” SPE Formation Evaluation, 189-193, September 1993.
6. Oren, P. E., and Pinczewski, W. V., “Fluid Distribution and Pore-Scalen Displacement Mechanisms in Drainage Dominated Three-Phase Flow,” Transport in Porous Media, 105-133, December 1995.
7. Rosenberg, E., Gueroult, P., Lynch, J., Bisiaux, M., and Ferreira De Paiva, R., “High Resolution Laboratory X-Ray Tomography on Rocks”, Society of core Analysts, 1997.
8. Al- Sharji H., Grattoni, C. A., Dawe, R. A., and Zimmerman, R., “Pore-scale Study of the Flow of Oil and Water through Polymer Gels,” SPE 56738, Proceedings, Annual Technical meeting, Houston, Texas, 3-6 October 1999.
9. Dullien, F. A., “Capillary Effects and Multiphase Flow in Porous Media,” Journal of Porous media, 1-29, January. 1977.
10. van Dijke, M. I. J., and Sorbie, K. S.: “An Analysis of Three-Phase Pore Occupancies and Relative Permeability in Porous Media with Variable Wettability,” Transport in Porous Media, August 2000.

11. Dicarlo, D., Sahni, A., and Blunt, M.: "Three-Phase Relative Permeability of Water–Wet, Oil Wet and Mixed-Wet Sandpacks," SPE Journal, 82-91, March 2000.
12. Wang, S. Y., Ayral, S., and Gryte, C. C., "Computed Tomography for the Observation of Oil Displacement in Porous Media," SPE Journal, 53-55, February 1984.
13. Wellington, S. L., Vinegar, H. J., "X-Ray Computerized Tomography," Journal of Petroleum Technology, 885-897, August 1987.
14. Hicks, P. J., Jr., Deans, H. A., and Narayama, K., "Distribution of Residual Oil Saturation on Heterogeneous Carbonate Cores Using X-Ray CT," SPE Journal, 235-239 September 1992.
15. Grader, A. S., and O'Meara, D. J., Jr., "Dynamic Displacement Measurements of Three-Phase Relative Permeabilities Using Three Immiscible Liquids," Proceedings, SPE Annual Meeting, 325-338, Huston, Texas, October. 1998.
16. Seright, R.S., Liang, J., Lindquist, W.B., and Dunsmuir, J.H., "Characterizing Disproportionate Permeability Reduction Using Synchrotron X-Ray Computed Microtomography" SPE Reservoir Evaluation and Engineering, 5, pp.355-364, 2002.